Earthquakes and Structures, *Vol. 10, No. 6 (2016) 1253-1272*
DOI: http://dx.doi.org/10.12989/eas.2016.10.6.1253

Robust market-based control method for nonlinear structure

Jian-Zhu Song[*1], Hong-Nan Li[1,2a] and Gang Li[1b]

[1]*State Key Lab of Coastal and Offshore Engineering, Liaoning Collaborative Innovation Center for Engineering Disaster Prevention and Mitigation, Dalian University of Technology, Dalian 116024, China*
[2]*School of Civil Engineering, Shenyang Jianzhu University, Shenyang 110168, China*

(Received December 17, 2015, Revised April 15, 2016, Accepted April 19, 2016)

Abstract. For a nonlinear control system, there are many uncertainties, such as the structural model, controlled parameters and external loads. Although the significant progress has been achieved on the robust control of nonlinear systems through some researches on this issue, there are still some limitations, for instance, the complicated solving process, weak conservatism of system, involuted structures and high order of controllers. In this study, the computational structural mechanics and optimal control theory are adopted to address above problems. The induced norm is the eigenvalue problem in structural mechanics, i.e., the elastic stable Euler critical force or eigenfrequency of structural system. The segment mixed energy is introduced with a precise integration and an extended Wittrick-Williams (W-W) induced norm calculation method. This is then incorporated in the market-based control (MBC) theory and combined with the force analogy method (FAM) to solve the MBC robust strategy (R-MBC) of nonlinear systems. Finally, a single-degree-of-freedom (SDOF) system and a 9-stories steel frame structure are analyzed. The results are compared with those calculated by the H∞ -robust (R-H∞) algorithm, and show the induced norm leads to the infinite control output as soon as it reaches the critical value. The R-MBC strategy has a better control effect than the R-H∞ algorithm and has the advantage of strong strain capacity and short online computation time. Thus, it can be applied to large complex structures.

Keywords: market-based control; force analogy method; robustness; extended W-W algorithm; precise integration method

1. Introduction

A precise process model is necessary for existing control strategies. However, there are usually many uncertainties in real nonlinear controlled systems, such as the unknown higher order, external load uncertainties and error of model parameters. The determination of a system matrix is not very accurate (Kuperman and Zhong 2011). Since 1950s, the control of uncertain nonlinear systems has attracted the attention of many researchers. The adaptive and robust controls are two main methods to solve these uncertainties and have been significantly improved. Based on the varied controlled objects and targets, there are different design tools in an nonlinear control

∗Corresponding author, Ph.D., E-mail: 215161086@qq.com
[a]Professor, E-mail: hnli@dlut.edu.cn
[b]Professor, E-mail: gli@dlut.edu.cn

http://www.techno-press.com/journals/eas&subpage=7 ISSN: 2092-7614 (Print), 2092-7622 (Online)

including the feedback linearization, variable structure control, non-source-based control, and back stepping (Aloliwi and Khalil 1997). Many adaptive control methods have been proposed to reduce the dependency of feedback linearization on the accurate mathematical models (Marino and Tomei 1997). The nonlinear adaptive control on nonparametric uncertainties prompted the development of robust adaptive control (Zhou and Wen 2011). The nonlinear robust control is proposed for the unmodeled dynamics and external disturbances in the uncertain nonlinear systems, considering the mathematical model and the worst effects of uncertainties on the performance of systems when designing controllers (Wang and Lin 2013). The design tools for the control method include differential geometry, small gain theorem, Lyapunov synthesis and non-source and dissipative approaches (Baskar and Bradley 1994, Cho *et al*. 2008, Luo and Sun 2015). The main research problems are robust stabilization of unmodeled dynamics and criterion design for the robust L_2 performance of external disturbance, i.e., the H_∞ robust control (Katebi *et al*. 1997). An adaptive robust control introduces the adaptive estimation of parameter uncertainties in the nonlinear robust control to reduce the conservatism of controllers for the expected control performance (Liu *et al*. 2009). If these uncertainties are not handled properly during the controller design process, the worse performance may result in the controlled system instable for the closed-loop system. Therefore, uncertainties of controlled object should be considered and is meaningful to design the controller based on the inaccurate models of uncertainties.

The market-based control (MBC) mechanism is a discrete control strategy (Lynch and Law 2002). And a complex control system is simulated by the market, in which the controllers and energy output are replaced respectively by sellers and consumers; therefore, the whole control system can be discretized. If the free market can rationally allocate resources, the control of vibration is also rational and effective by analogy. The MBC strategy is first applied to the structural vibration control in civil engineering by Lynch and Law (2002). The method describes the derivation of energy market-based control (Lynch and Law 2004), a decentralized approach that models the structural control system as a competitive marketplace. At present, the most of studies on the MBC focus on linear structures; for example, Huo and Li (2005) applied the MBC to the semi-active TLCD control and proposed a new semi-active TLCD control scheme based on the market mechanisms. the MBC strategy was applied to the semi-active vibration isolation system and put forward to the corresponding control strategy (Li and Li 2008), Which effectively controlled the MRD voltage in real time. However, the research on the MBC robust theory is quite few.

The local damage, overload and other initial faultiness should be considered in the robust analysis for structures because they often enter plastic state when subjected to strong earthquakes. Conventional nonlinear analytical methods are time consuming. However, the force analogy method (FAM) is an efficient nonlinear analysis method (Lin and Pian 1969) that has been applied to the seismic analysis for engineering structures in recent years. The basic assumption is that when the structure enters the nonlinear stage, the plastic deformation occurs at certain locations while the rest of components remain elastic. The performance of local positions can be described by the plastic hinge, the rotation of which causes the plastic displacement of structures. The core step of the FAM is to assume that the plastic hinge is an ideal one under the bending moment and thus the nonlinear solving process is obtained through the relationship between the plastic hinge and the restoring force of structure. The FAM was applied to a nonlinear prediction optimization control (Wong 2005), in which the time delay of active control was well solved owing to the fast response of the FAM. A computational approach was proposed to study the potential energy of fully nonlinear framed structures and other energy characteristics due to earthquake ground motions (Wong and Zhao 2007). The method uncoupled the geometric nonlinearity and material inelasticity effects before solving the motion equation, which directly led to the analytical representations of each energy form. With the consideration of full-range behaviors including the material and geometric nonlinearity, stiffness degradation, strength degradation, and the failure of RC members, Li *et al*. (2014) developed a procedure of nonlinear dynamic analysis of RC framed structures based on the FAM. Unlike the conventional varied stiffness method, the FAM requires less storage space and computational time. If the local deformation state can be captured, the overall deformation information will be obtained to realize the solution of the nonlinear deformation. Further, a new method that combined the linear MBC strategy and the FAM was presented to realize the nonlinear structural vibration control (Li *et al*. 2010), and the effectiveness of the strategy was testified through numerical examples. Moreover, the MBC robust strategy can be combined with the FAM to solve the robust control problems for nonlinear structures.

The H_∞ control strategy for linear systems has been achieved with great progress through recent researches on theory and experiments, such as the linear matrix inequalities (LMI) method (Zhang 2004), differential game method (Kushner 2006), μ analysis and μ comprehensive method (Safonov 2012). However, these methods have the limitation of a complicated solving process, weak conservatism, complex structures and a high-order controller. The uncertainties in the controlled system can be expressed by the induced norm in mathematics. The literature (Zhong *et al*. 1997, Wu and Zhong 2009, Peng *et al*. 2014) introduced the segment mixed energy to solve the critical value of induced norm γ_{cr}^{-2} with a precise integration and extended W-W algorithm from a new perspective for a H_∞ robust controller. They also proved that the solution could be as precise as computers in theory. However, since the H_∞ control requires full state information and solving a complicated Riccati equation, it needs the long online time. The MBC requires only the state information of discrete points and has the advantage of short online time and easy selection of parameters.

The present study uses the computational structural mechanics and optimal control theory to address the existing problems. The induced norm is the eigenvalue problem in structural mechanics, i.e., the elastic stable Euler critical force or eigenfrequency of structural vibrations (Wu and Zhong 2009). The precise integration and extended Wittrick-Williams method are used to calculate the induced norm. As for high-rise shear type structures, the MBC robust control for nonlinear structures (R-MBC) is proposed by introducing the induced norm into the MBC theory to solve nonlinear parts of structures with the FAM. Finally, a single-degree-of-freedom systems and a 9-layer steel frame structure are analyzed and results are compared with those calculated by the H_∞ robust (R-H_∞) algorithm, and show that the induced norm leads to the infinite control output as soon as it reaches the critical value. The R-MBC strategy has a better control effect than the R-H_∞ algorithm and has the advantage of strong strain capacity and short online computation time. Thus, it can be applied to large complex structures.

2. Principle of MBC

2.1 Supply and demand functions

The MBC applies the free market competition mechanism to the control system since it has a certain similarity to the market. Compared with a free market economy in which goods owned by a seller are scarce resources to be allocated, in the control system, the controlled energy required by the controlled structure (led by control device output) is a scarce resource to be allocated (Lynch and Law 2004). The key problem with the MBC algorithm in the field of engineering control is to determine the demand equation of the controlled structure, i.e., the consumer with respect to the control device. The proper selection of demand equation has great influence on the quality of control system.

When using the market mechanisms to simulate the structure of control system, the supply and demand function of virtual market does not have a strict form. The market price, as a primary consideration when selecting the supply function, means that the higher prices lead to the greater supply. The selection of demand function lies in the consideration of response of structure and the price of control energy, which means that the higher the prices, the less the structures tend to be purchased, and vice versa. The present study pays attention to effects of nonlinear control. The plastic deformation of structure must be considered when constructing a functional supply and demand model. The MBC multi-market strategy model can be derived as follows.

The control energy demand of the *i*-story ($\boldsymbol{Q}_{Di,j}$) in the *j*th submarket has a relationship with the inter-story displacement ($\boldsymbol{x}_{di,j}$), inter-story velocity ($\dot{\boldsymbol{x}}_{di,j}$), wealth ($\boldsymbol{W}_{i,j}$) and price ($\boldsymbol{p}_j$), which can be expressed by

$$\boldsymbol{Q}_{Di,j} = f(\boldsymbol{x}_{di,j}, \dot{\boldsymbol{x}}_{di,j}, \boldsymbol{W}_{i,j}, \boldsymbol{p}_j) \tag{1}$$

The energy supply of the *k*th control energy source in the *j*th submarket ($\boldsymbol{Q}_{Sk,j}$) related with the market price and elastic displacement can be given by

$$\boldsymbol{Q}_{Sk,j} = f(\boldsymbol{p}_j) \tag{2}$$

When the supply and demand in the sub-market reaches to equilibrium

$$\sum_i \boldsymbol{Q}_{Di,j} = \sum_k \boldsymbol{Q}_{Sk,j} \tag{3}$$

where the equilibrium price $\boldsymbol{p}_j$ of the *j*th market can be obtained by combining Eqs. (1)-(3), which is called a Pareto optimization solution. This can be substituted into Eq. (2) to obtain the control energy needed for each story. That is, in each time step, the equilibrium price of each market can be solved according to the equal control energy and demand energy. The energy distribution is globally optimal at this moment. In the meantime, the Pareto optimal solution itself is a static optimization solution, which is equivalent to a dynamic optimization solution because it is distributed discretely in time.

2.2 Force analogy method (FAM)

Compared with the conventional nonlinear analysis method, the stiffness matrices are unchanged throughout the computational process. The basic theory of the FAM is to decompose the structural state as a superposition of elastic and plastic states; at the same time, the displacement of the structure is divided into the elastic and plastic displacements (Lin and Pian 1969, Wong 2005, Wong and Zhao 2007, Li *et al*. 2014).When the constitutive relation of structures is then broken lines shown in Fig. 1 (Li *et al*. 2011), the elastic line of OA is firstly extended, then the force $\boldsymbol{F}(t)$ is intersected at point B, so the abscissa of point B is the elastic displacement. Therefore, the displacement of structures can be represented as

$$\boldsymbol{x}(t) = \boldsymbol{x}'(t) + \boldsymbol{x}''(t) \tag{4}$$

where $\boldsymbol{x}(t)$, $\boldsymbol{x}'(t)$ and $\boldsymbol{x}''(t)$ represent the total displacement, elastic displacement and plastic displacement, respectively.

Assume that the plastic deformation, i.e., the plastic rotation here, is generated at the end of the structural members. The relationship between the force and displacement for structural members is converted to the relationship between the internal force and plastic deformation of the plastic hinge. To be consistent with the displacement components, the moment of the plastic hinge $\boldsymbol{M}(t)$ is expressed as elastic $\boldsymbol{M}'(t)$ and plastic $\boldsymbol{M}''(t)$ (Li *et al*. 2011) as

$$\boldsymbol{M}(t) = \boldsymbol{M}'(t) + \boldsymbol{M}''(t) \tag{5}$$

After a series of derivations (Wong 2005), Eq. (5) can be rewritten by

$$\boldsymbol{M}(t) = \boldsymbol{K}_P^T \boldsymbol{x}(t) - \boldsymbol{K}_R \boldsymbol{\theta}''(t) \tag{6}$$

and

$$\boldsymbol{F}(t) = \boldsymbol{K}\boldsymbol{x}'(t) = \boldsymbol{K}(\boldsymbol{x}(t) - \boldsymbol{x}''(t)) = \boldsymbol{K}\boldsymbol{x}(t) - \boldsymbol{K}_P \boldsymbol{\theta}''(t) \tag{7}$$

where $\boldsymbol{K}$ is the elastic stiffness matrix of structure, $\boldsymbol{K}_R$ is the stiffness matrix related to the plastic rotation $\boldsymbol{\theta}''(t)$ with the moment at the plastic hinge, and $\boldsymbol{K}_p$ is the stiffness matrix related to the plastic rotation $\boldsymbol{\theta}''(t)$ with the resorting force.

When the external forces are known, Eqs. (6)-(7) include three unknown variables $\boldsymbol{M}(t)$, $\boldsymbol{x}(t)$ and $\boldsymbol{\theta}''(t)$. A supplementary relationship must be established to solve the above equations. This relationship can be established through the plastic hinge moment $\boldsymbol{M}''(t)$ and plastic rotation $\boldsymbol{\theta}''(t)$ as shown in Fig. 2.

The hysteretic relationship of plastic hinge is the strengthening of the rigid hinge curves (Wong and Zhao 2007)

$$\boldsymbol{M} = \boldsymbol{f}(\boldsymbol{\theta}'') = \begin{cases} \boldsymbol{M}_y + \boldsymbol{k}_t \boldsymbol{\theta}'' & \boldsymbol{M} \geq \boldsymbol{M}_y, \quad \boldsymbol{\theta}'' \neq 0 \\ \boldsymbol{M} & \boldsymbol{M} < \boldsymbol{M}_y, \quad \boldsymbol{\theta}'' = 0 \end{cases} \tag{8}$$

where $\boldsymbol{M}_y$ is the yield moment, and $\boldsymbol{k}_t$ is the strengthening stiffness.

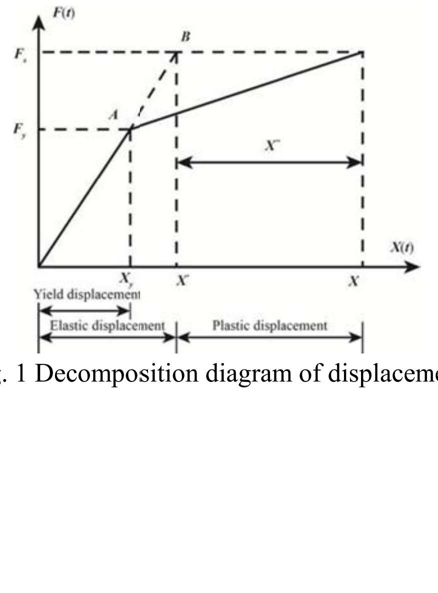

Fig. 1 Decomposition diagram of displacement

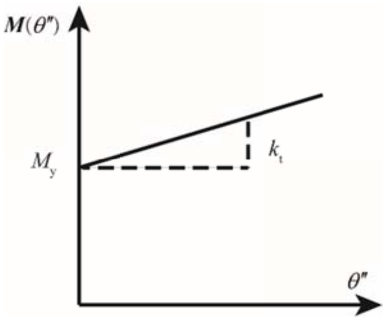

(a) Strengthening rigid hinge

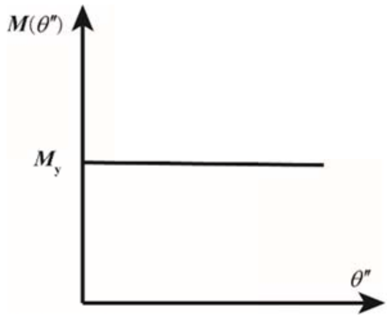

(b) Normal rigid hinge

Fig. 2 Relationship of rotation of rigid hinge versus moment

3. Controller design of robust MBC

This section illustrates robust market-based control method for nonlinear structure. The first part is the controller design process and the second part is the solution for induced norm.

3.1 Robust MBC method

The MBC robust controller for a nonlinear structure is designed based on the characteristics of robust control and the force analogy method. System matrix $\boldsymbol{A}$ is the law of reflection of motion for the controlled object. In practice, some errors are inevitably introduced by abstraction. The robust control considers the changing matrix $\Delta\boldsymbol{A}$ that varies in a given range and chooses the most adverse change matrix. Considering the factor, the dynamic equation and equation of structure based on the FAM is converted to

$$\dot{\boldsymbol{Z}}(t) = \boldsymbol{A}\boldsymbol{Z}(t) + (\Delta\boldsymbol{A}\boldsymbol{Z} + \boldsymbol{B}_w\boldsymbol{w}) + \boldsymbol{B}_{\mathrm{u}}\boldsymbol{U}(t) + \boldsymbol{F}_p^c(t)\boldsymbol{x}''(t) \tag{9}$$

$$\boldsymbol{Y} = \boldsymbol{C}_Z\boldsymbol{Z} + \boldsymbol{D}_{\mathrm{u}}\boldsymbol{U} \tag{10}$$

where $\boldsymbol{Z}(t) = \begin{Bmatrix} \boldsymbol{x}(t) \\ \dot{\boldsymbol{x}}(t) \end{Bmatrix}$; $\boldsymbol{A} = \begin{bmatrix} \boldsymbol{0} & \boldsymbol{I} \\ -\boldsymbol{M}^{-1}\boldsymbol{K} & -\boldsymbol{M}^{-1}\boldsymbol{C} \end{bmatrix}$; $\boldsymbol{B}_u = \begin{bmatrix} \boldsymbol{0} \\ \boldsymbol{M}^{-1}\boldsymbol{B}_s \end{bmatrix}$; $\boldsymbol{B}_w = \begin{bmatrix} \boldsymbol{0} \\ -\boldsymbol{I} \end{bmatrix}$; $\boldsymbol{F}_p^c = \begin{bmatrix} \boldsymbol{0} \\ \boldsymbol{M}^{-1}\boldsymbol{K} \end{bmatrix}$; $\boldsymbol{M}$, $\boldsymbol{C}$ and $\boldsymbol{K}$ are the mass, stiffness and damping matrices of system, respectively; $\boldsymbol{x}(t)$ and $\dot{\boldsymbol{x}}(t)$ are the displacement and velocity vectors with n dimensions; $\boldsymbol{x}''(t)$ is the plastic displacement; $\boldsymbol{w}$ is the white noise vector; $\boldsymbol{B}_w$ and $\boldsymbol{B}_{\mathrm{u}}$ are the external interference position and force matrices; $\boldsymbol{U}(t)$ is the control force vector; $\boldsymbol{Y}(t)$ is the output vector; and $\boldsymbol{C}_z$ and $\boldsymbol{D}_u$ are the output and transfer matrices, respectively. There are following relations as (Peng *et al*. 2014)

$$\boldsymbol{D}_{\mathrm{u}}^{\mathrm{T}}\boldsymbol{D}_{\mathrm{u}} = \boldsymbol{I}_m \tag{11}$$

The precise expression of robust control can be described by introducing the induced norm. The worst disturbance to the system should be considered by combining $\Delta\boldsymbol{A}$ with the disturbance term in Eq. (9) and meeting the requirement of system robustness. H$_\infty$ norm (γ^2), which denotes the anti-jamming performance, is introduced in the robust control system. When $\boldsymbol{B}_w\boldsymbol{w}$ trends to zero, that is, the external disturbance is produced entirely by $\Delta \boldsymbol{A}$, one can obtain a critical value γ_{cr}^2 according to Eq. (14), which is the value at which the system can excite itself when there are no external excitations. This norm represents the optimal anti-jamming performance which can reach to, and the control system generally takes the suboptimal value (which satisfies that $\gamma^2 > \gamma_{cr}^2$) to design. When γ^2 is larger than γ_{cr}^2, the system will not lose stability because of $\boldsymbol{w}$; that is, the system can bear an external disturbance and is stable. $\boldsymbol{Y}$ can be quantified by its norm; i.e.

$$\|\boldsymbol{Y}\| = \int_t^{t_f} \boldsymbol{Y}^{\mathrm{T}}\boldsymbol{Y}/2\mathrm{d}\tau + \boldsymbol{Z}_f^{\mathrm{T}}\boldsymbol{S}_f\boldsymbol{Z}_f/2, \min_{\boldsymbol{U}}\|\boldsymbol{Y}\| \tag{12}$$

where

$$\|\boldsymbol{w}\| = \int_t^{t_f} \boldsymbol{w}^{\mathrm{T}}\boldsymbol{w}/2\mathrm{d}\tau \tag{13}$$

Considering the most disadvantageous disturbance, the excitation $\boldsymbol{w}$ should be set to maximize $\|\boldsymbol{Y}\|$ (Tan *et al*. 2008)

$$\gamma^2 = \|\boldsymbol{Y}\|/\|\boldsymbol{w}\|, \max_{\boldsymbol{w}} \min_{\boldsymbol{U}} \gamma^2 = \gamma_{cr}^2 \tag{14}$$

The extreme value of induced norm is a variation problem and satisfies the dynamic equation and output equation, so the problem is conditional variation. Eq. (14) can be changed to

$$J_c = \int_t^{t_f} (\boldsymbol{Y}^{\mathrm{T}}\boldsymbol{Y}/2 - \gamma^2 \boldsymbol{w}^{\mathrm{T}}\boldsymbol{w}/2)\mathrm{d}\tau + \boldsymbol{Z}_f^{\mathrm{T}}\boldsymbol{S}_f\boldsymbol{Z}_f/2, \max_{\boldsymbol{w}} \min_{\boldsymbol{U}} J_c \tag{15}$$

By substituting Eq. (9) into Eq. (15) and introducing Lagrange parameter vector λ, one can obtain

$$\begin{aligned} J_{cA} = \int_t^{t_f} (&\boldsymbol{\lambda}^{\mathrm{T}}(\dot{\boldsymbol{Z}} - \boldsymbol{AZ} - \boldsymbol{B}_w\boldsymbol{w} - \boldsymbol{B}_{\mathrm{u}}\boldsymbol{U} - \boldsymbol{F}_p^c(t)\boldsymbol{x}''(t)) + \boldsymbol{U}^{\mathrm{T}}\boldsymbol{U}/2 + \boldsymbol{U}^{\mathrm{T}}\boldsymbol{D}_{\mathrm{u}}^{\mathrm{T}}\boldsymbol{C}_z\boldsymbol{Z} + \boldsymbol{Z}^{\mathrm{T}}\boldsymbol{C}_z^{\mathrm{T}}\boldsymbol{C}_z\boldsymbol{Z}/2) \\ &-\gamma^2 \boldsymbol{w}^{\mathrm{T}}\boldsymbol{w}/2)\mathrm{d}\tau + \boldsymbol{Z}_f^{\mathrm{T}}\boldsymbol{S}_f\boldsymbol{Z}_f/2, \delta J_{cA} = 0 \end{aligned} \tag{16}$$

where J_{cA} is the extended indicator functional, which has four types of variables. By selecting the maximum of w and minimum of $\boldsymbol{U}$ for J_{cA}, one can obtain

$$\frac{\delta \boldsymbol{J}_{cA}}{\delta \boldsymbol{w}} = \boldsymbol{0}, \ \boldsymbol{w} = -\gamma^2\boldsymbol{B}_w^{\mathrm{T}}\lambda \tag{17}$$

$$\frac{\delta \boldsymbol{J}_{cA}}{\delta \boldsymbol{U}} = \boldsymbol{0}, \ \boldsymbol{\lambda} = (\boldsymbol{B}_{\mathrm{u}}^{\mathrm{T}})^{-1}(\boldsymbol{U} + \boldsymbol{D}_{\mathrm{u}}^{\mathrm{T}}\boldsymbol{C}_z\boldsymbol{Z}) \tag{18}$$

Set the stationary value of J_{cA} equaling to $\boldsymbol{\lambda}$ in Eq. (16), and substituting Eq. (17) into Eq. (18) yields

$$\dot{\boldsymbol{Z}}(t) = \tilde{\boldsymbol{A}}\boldsymbol{Z}(t) + \tilde{\boldsymbol{B}}\boldsymbol{U}(t) + \boldsymbol{F}_p^c(t)\boldsymbol{x}''(t) \tag{19}$$

where $\tilde{\boldsymbol{A}} = \boldsymbol{A} - \gamma^{-2}\boldsymbol{B}_w\boldsymbol{B}_w^{\mathrm{T}}(\boldsymbol{B}_{\mathrm{u}}^{\mathrm{T}})^{-1}\boldsymbol{D}_{\mathrm{u}}^{\mathrm{T}}\boldsymbol{C}_z$, $\tilde{\boldsymbol{B}} = \boldsymbol{B}_{\mathrm{u}} - \gamma^{-2}\boldsymbol{B}_w\boldsymbol{B}_w^{\mathrm{T}}(\boldsymbol{B}_{\mathrm{u}}^{\mathrm{T}})^{-1}$.

The present study uses an exponent supply and demand function model (Li and Li 2008), whose control force can be expressed by

$$\boldsymbol{U} = -Q \cdot \boldsymbol{W} \cdot (\boldsymbol{\alpha x}_{d,i} + \boldsymbol{\beta \dot{x}}_{d,i}) \cdot e^{-cp} \tag{20}$$

where c is the demand adjustment coefficient that can be set to 1, p is the equilibrium price of control energy, $\boldsymbol{\alpha}$ and $\boldsymbol{\beta}$ are the corresponding algorithm stability parameters, $\boldsymbol{x}_{d,i}$ and $\dot{\boldsymbol{x}}_{d.i}$ are the inter-story drift and velocity of system, respectively; $\boldsymbol{W}$ is the wealth of control devices, and Q is the gain coefficient.

The parameters for the control force are selected based on the following procedure: four earthquake waves are used to perform the dynamic analysis of an uncontrolled structure. Calculate the average of the story drift and inter-story peak velocity of uncontrolled structures when subjected to these ground motions. Normalize the two average values, i.e., $\boldsymbol{\alpha}$ and $\boldsymbol{\beta}$. Finally, choose the control gain factor Q according to the output force range of control device.

3.2 Computation of optimal induced norm

In Eq. (19), the extra term γ^{-2} in the system matrix is the characteristic of robust control. When γ^{-2} tends to zero, it is the MBC algorithm. The external disturbance is caused entirely by $\Delta\boldsymbol{A}$, which means that the deviation of $\boldsymbol{A}$ causes the disturbance. When γ^{-2} increases, $\Delta\boldsymbol{A}$ has a great impact on the stability. However, over large γ_{cr}^{-2} will leads to the system instability. Thus, the critical value of γ_{cr}^{-2} is worthy to discuss.

According to structural mechanics and optimal control theory, the induced norm γ^2 is the eigenvalue problem in the structural mechanics, i.e., the elastic stable Euler critical force or the eigen-frequency of structural vibration (Zhong *et al*. 1997, Zhong 2004, Tan *et al*. 2008, Peng *et al*. 2014). According to the extended Wittrick-Williams (W-W) algorithm, the precise integration can be solved for the critical parameter γ_{cr}^{-2}. The integration divides a time step η into $\tau=2^N$ sub-steps, and N can be approximately.

The variational Eq. (16) can be expressed by

$$J_{cA} = \int_t^{t_f} (\boldsymbol{\lambda}^{\mathrm{T}}\dot{\boldsymbol{Z}} - V(\boldsymbol{Z},\boldsymbol{\lambda}) + \boldsymbol{F}_p^c(t)\boldsymbol{x}''(t))\mathrm{d}\tau + \boldsymbol{Z}_f^{\mathrm{T}}\boldsymbol{S}_f\boldsymbol{Z}_f/2 \tag{21}$$

where

$$V(\boldsymbol{Z},\boldsymbol{\lambda}) = \boldsymbol{\lambda}^{\mathrm{T}}(\boldsymbol{B}_{\mathrm{u}}\boldsymbol{B}_{\mathrm{u}}^{\mathrm{T}} - \gamma^{-2}\boldsymbol{B}_w\boldsymbol{B}_w^{\mathrm{T}})\boldsymbol{\lambda}/2 + \boldsymbol{\lambda}^{\mathrm{T}}(\boldsymbol{A} - \boldsymbol{B}_{\mathrm{u}}\boldsymbol{D}_{\mathrm{u}}^{\mathrm{T}}\boldsymbol{C}_z)\boldsymbol{Z} - \boldsymbol{Z}^{\mathrm{T}}\boldsymbol{C}_z^{\mathrm{T}}(\boldsymbol{I} - \boldsymbol{D}_{\mathrm{u}}\boldsymbol{D}_{\mathrm{u}}^{\mathrm{T}})\boldsymbol{C}_z\boldsymbol{Z}/2 \tag{22}$$

Define the interval (k, k+1) mixed energy

$$V(\boldsymbol{Z}_a,\boldsymbol{\lambda}_b) = \boldsymbol{\lambda}_b^{\mathrm{T}}\boldsymbol{F}\boldsymbol{Z}_a + \boldsymbol{\lambda}_b^{\mathrm{T}}\boldsymbol{G}\boldsymbol{\lambda}_b/2 - \boldsymbol{Z}_a^{\mathrm{T}}\boldsymbol{Q}\boldsymbol{Z}_a/2 \tag{23}$$

where $\boldsymbol{F} = \boldsymbol{A} - \boldsymbol{B}_{\mathrm{u}}\boldsymbol{D}_{\mathrm{u}}^{\mathrm{T}}\boldsymbol{C}_z$, $\boldsymbol{G} = \boldsymbol{B}_{\mathrm{u}}\boldsymbol{B}_{\mathrm{u}}^{\mathrm{T}} - \gamma^{-2}\boldsymbol{B}_w\boldsymbol{B}_w^{\mathrm{T}}$ and $\boldsymbol{Q} = \boldsymbol{C}_z^{\mathrm{T}}(\boldsymbol{I} - \boldsymbol{D}_{\mathrm{u}}\boldsymbol{D}_{\mathrm{u}}^{\mathrm{T}})\boldsymbol{C}_z$.

The importance of the interval mixed energy is that two consecutive intervals (t_{a}, t_{b}) and (t_{a}, t_{c}) can be combined into a longer interval (t_{a}, t_{c}), whose interval mix energy is

$$V(\boldsymbol{Z}_{\mathrm{a}},\boldsymbol{\lambda}_{\mathrm{c}}) = \boldsymbol{\lambda}_{\mathrm{c}}^{\mathrm{T}}\boldsymbol{F}\boldsymbol{Z}_{\mathrm{a}} + \boldsymbol{\lambda}_{\mathrm{c}}^{\mathrm{T}}\boldsymbol{G}\boldsymbol{\lambda}_{\mathrm{c}}/2 - \boldsymbol{Z}_{\mathrm{a}}^{\mathrm{T}}\boldsymbol{Q}\boldsymbol{Z}_{\mathrm{a}}/2 \tag{24}$$

where

$$\boldsymbol{Q}_c = \boldsymbol{Q}_1 + \boldsymbol{F}_1^{\mathrm{T}}(\boldsymbol{Q}_2^{-1} + \boldsymbol{G}_1)^{-1}\boldsymbol{F}_1 \tag{25}$$

$$\boldsymbol{G}_c = \boldsymbol{G}_2 + \boldsymbol{F}_2(\boldsymbol{G}_1^{-1} + \boldsymbol{Q}_2)^{-1}\boldsymbol{F}_1 \tag{26}$$

$$\boldsymbol{F}_c = \boldsymbol{F}_2(\boldsymbol{I} + \boldsymbol{G}_1\boldsymbol{Q}_2)^{-1}\boldsymbol{F}_1 \tag{27}$$

A given parameter $\gamma_{\#}^{-2} = \omega_{\#}^2$ (Zhong *et al*. 1997), when the displacement is zero at the left end and the force is zero at the right end of segment (t_a, t_b), $J_R(\omega_{\#}^2)$ is the count of eigenvalue $\omega^2 < \omega_{\#}^2$ in the segment, i.e., the count of the eigenvalue for $\gamma_{cr}^{-2} < \gamma_{\#}^{-2}$

$$J_{Rc}(\omega_{\#}^2) = J_{R1}(\omega_{\#}^2) + J_{R2}(\omega_{\#}^2) - \mathrm{s}\{\boldsymbol{Q}_2\} + \mathrm{s}\{\boldsymbol{G}_1 + \boldsymbol{Q}_2^{-1}\} \tag{28}$$

where J_{R1} and J_{R2} are the numbers of eigenvalues that are smaller than $\omega_{\#}^2$ for segment 1 and

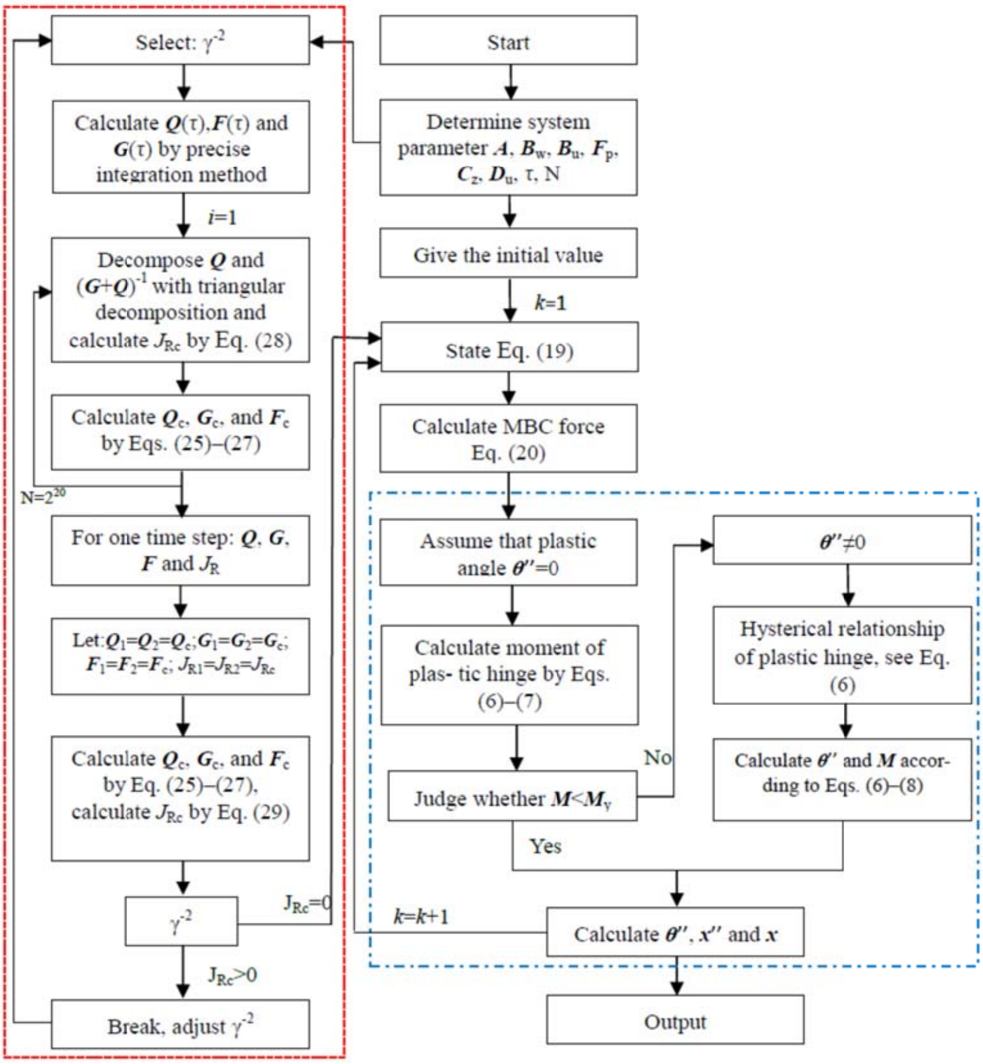

Fig. 3 Design process of MBC robust controller for nonlinear structures

segment 2, J_{Rc} is the number of eigenvalues smaller than $\omega_{\#}^{2}$ when segment 1 and segment 2 are combined, and $\mathrm{s}\{\boldsymbol{M}\}$ is the number of negative numbers when $\boldsymbol{M}$ is decomposed into the triangulation form of symmetrical matrix $\boldsymbol{M}$ by $\boldsymbol{M} = \boldsymbol{LDL}^{\mathrm{T}}$.

The number of eigenvalues for the whole segment can be expressed by

$$J_{Rf} = J_R - \mathrm{s}\{\boldsymbol{S}_f\} + \mathrm{s}\{\boldsymbol{G} + \boldsymbol{S}_f^{-1}\} \tag{29}$$

$\gamma_{\#}^{-2}$ is then a suboptimal parameter if $J_{Rf} = 0$, which means that there is no singularity point in the whole segment. For any given precision of the eigenvalue of γ_{cr}^{-2}, it can be determined when searching for $\gamma_{\#}^{-2}$. The segment matrixes $\boldsymbol{F}$, $\boldsymbol{G}$ and $\boldsymbol{Q}$ in the mixed energy can be calculated by the precise integration (Zhong 2004). Fig. 3 shows the design process of the MBC robust controller for the nonlinear structures, where the process on the left with the dotted box is the W-W algorithm for the induced norm, and the process on the right with the dot-dash line box is the FAM.

4 **Numerical examples**

4.1 A single-degree-of-freedom structure

To verify the effectiveness of robust MBC for a nonlinear structure controller, a numerical analysis is conducted for a single-degree-of-freedom structure (Li *et al*. 2014). The model has the following characteristics: the span of 2.5 m and height of 2.5 m. Assume that four plastic hinge locations (PHLs) exist in this frame: two at the two ends of the beam and two at the bottom end of the two columns. The sketch and PHL numbers of structure are shown in Figs. 4 and 5. The floor masses are assumed to be 16,000 kg, and the other structural parameters are shown in Table 1. The ground motion of El Centro is selected as the excitation input with the peak ground acceleration (PGA) scaled to 500 gal with the duration of 20 s.

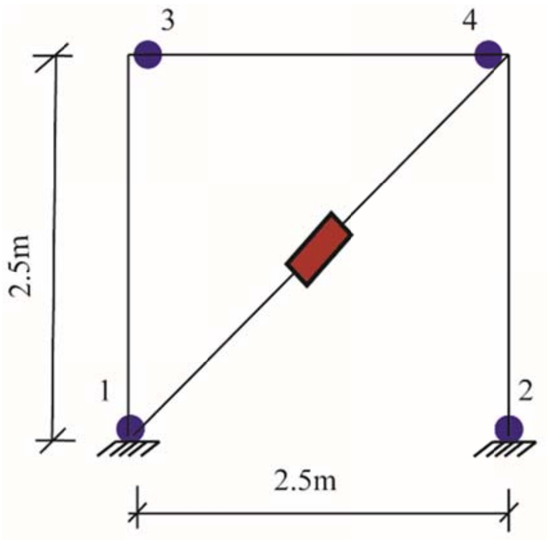

Fig.4 Distribution of the plastic hinges

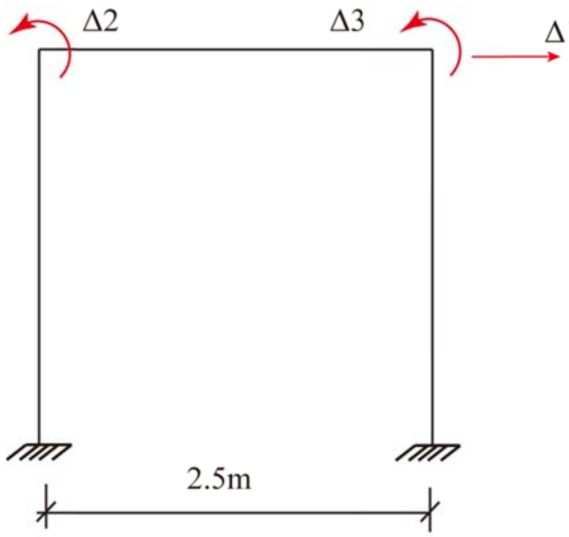

Fig. 5 Numeration of structural degree of freedom

Table 1 Main parameters of structure

Structural component	Elastic modulus EI (N×m^2)	Yielding moment M(N×m)
1st rows columns	2.87×10^6	3.107×10^5
1st rows beams	2.87×10^6	3.107×10^5

Table 2 Main parameters of magnetorheological damper

Diameter of cylinder (mm)	Effective length of piston (mm)	Diameter of piston rod (mm)	Gap spacing (mm)	Performance liquid viscosity(Pa·s)	Fluid maximum yield stress (kPa)
250	300	60	2	1	50

The structure is controlled by an MRD control device, the calculation model of MRD is the shear valve type, the damping force is from 23 kN to 1200 kN, and its parameters are listed in Table 2. The semi-active control law uses the corrected limited boundary Hrovat algorithm (Hrovat *et al*. 2014)

$$u_{\mathrm{d}} = \begin{cases} c_{\mathrm{d}}\dot{x} + f_{\mathrm{d,min}}\,\mathrm{sgn}(\dot{x}), u\dot{x} \geq 0 \\ |u|\,\mathrm{sgn}(\dot{x}), \qquad u\dot{x} < 0, |u| < u_{\mathrm{d,max}} \\ c_{\mathrm{d}}\dot{x} + f_{\mathrm{d,max}}\,\mathrm{sgn}(\dot{x}), u\dot{x} < 0, |u| > u_{\mathrm{d,max}} \end{cases} \tag{30}$$

where $\dot{x}$ is the story velocity, and $u_{\mathrm{d,max}} = c_{\mathrm{d}}\dot{x} + f_{\mathrm{d,max}}$, in which $u_{\mathrm{d,max}} = c_{\mathrm{d}}\dot{x} + f_{\mathrm{d,min}}$ are the maximum and minimum damping forces from MRD at any time, respectively.

The parameters of controller can be obtained from Eq. (20) as: the gain factor K=700000, $\boldsymbol{\alpha}$=diag([0, 0.0057]) and $\boldsymbol{\beta}$=diag(0.573, 0.571]). The critical value of the induced norm for the uncertain part of the system can be determined according to the extended W-W algorithm, i.e., Eqs. (21)-(29) and the value equals to 8.32. In practice, the optimal value is the critical value by 0.3 times. Fig. 6(a) and 6(b) show the relative displacement and control force for different values of parameter γ, respectively. It can be seen that when parameter γ^{-2} is close to the critical value, the control effect becomes worse and requires the greater control force.

Fig. 7 shows the moment of the No.2 plastic hinge and hysterical relationship of the plastic rotation wave, and Fig. 8 displays the time history of the plastic rotation of the No.2 hinge when subjected to the El Centro earthquake. FREE represents uncontrolled and R-MBC represents the robust MBC for nonlinear structures designed by the present study. It can be seen that the structure enters a plastic state without any control. The FAM performs well in the dynamic nonlinear analysis of structure, and the R-MBC strategy reveals a good performance in the nonlinear control of structure.

Table 3 shows the peak response and control effect under different cases when subjected to the El Centro earthquake wave. It can be concluded that the response of the R-MBC strategy is smaller than that of the N-MBC strategy because the R-MBC considers the uncertainty of system when the control force parameters are the same. The uncertainty means that the system matrix is varied. Therefore, the responses of structure are different between the two cases, which demonstrate the importance of considering the robustness for the controlled system. Moreover, the R-MBC strategy designed by the present study achieved a good control effect for structure. For example, the relative displacement of the 1$^{\text{st}}$ floor decreased by 70.75%, and the absolute

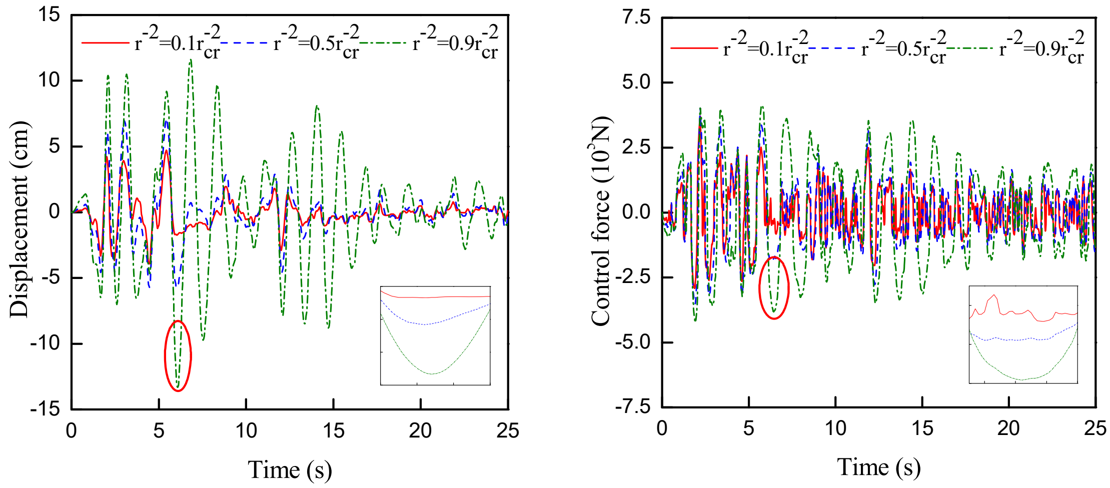

(a) Inter-story displacement (b) Control force

Fig. 6 Time history of relative displacement and control force under different *γ*

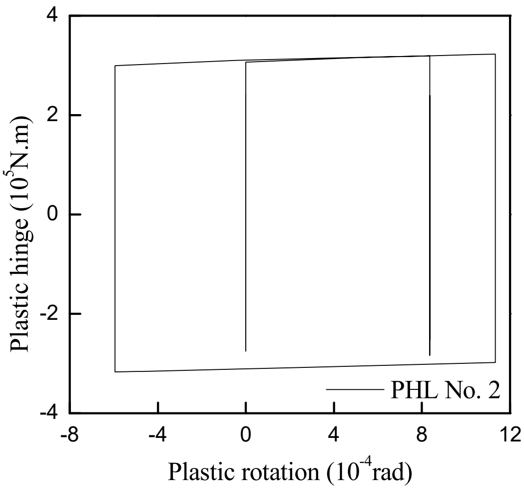

Fig.7 Relationship of rotation of rigid hinge versus moment No.2 plastic hinge

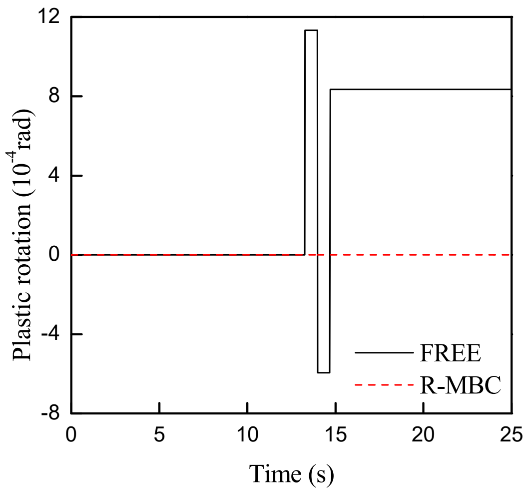

Fig.8 Rotation curves versus time history of the 2nd PHL

acceleration decreased by 39.72%. To demonstrate the importance of robustness analysis, Fig. 9 shows the displacement time history of first floor under the El Centro seismic excitation.

Fig. 10 shows the damper output force against the structural response, in which the control force is output in the form of damping force because the variable damping is of characteristic of MRD, and the force is in the opposite direction to the relative velocity. Fig. 11 shows the response of price and wealth of the virtual market in the controlled time. Compared to the ground motion time history, the price has the same variation trend as the input ground motions for every algorithm, which indicates that the price mechanism and wealth distribution reflect the variation of the needed control force and the impact of input on the output force of the controlled system when the structure is subjected to an earthquake wave.

Table 3 Peak response and control effect under different cases when subjected to El Centro earthquake wave

Earthquake	Cases	Absolute displacement		Absolute acceleration	
		Peak (cm)	Reduction rate (%)	Peak (m/s^2)	Reduction rate (%)
El Centro	FREE	20.0	—	7.15	—
	N-MBC	13.34	33.3	6.38	10.77
	R-MBC	5.85	70.75	4.31	39.72

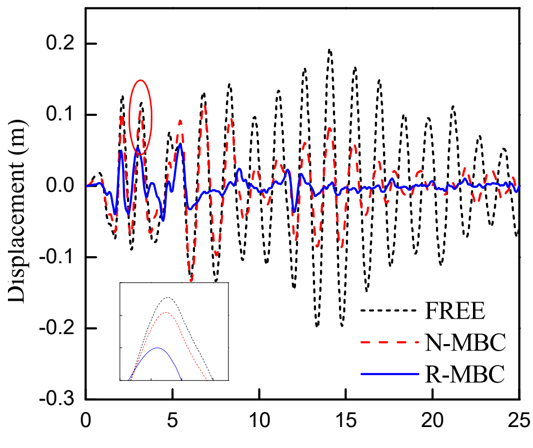

Fig. 9 Displacement time history of first floor under El Centro seismic excitation (Note: FREE represents uncontrolled, N-MBC represents the MBC algorithm without the robustness factor, and R-MBC represents the robust MBC for nonlinear structures)

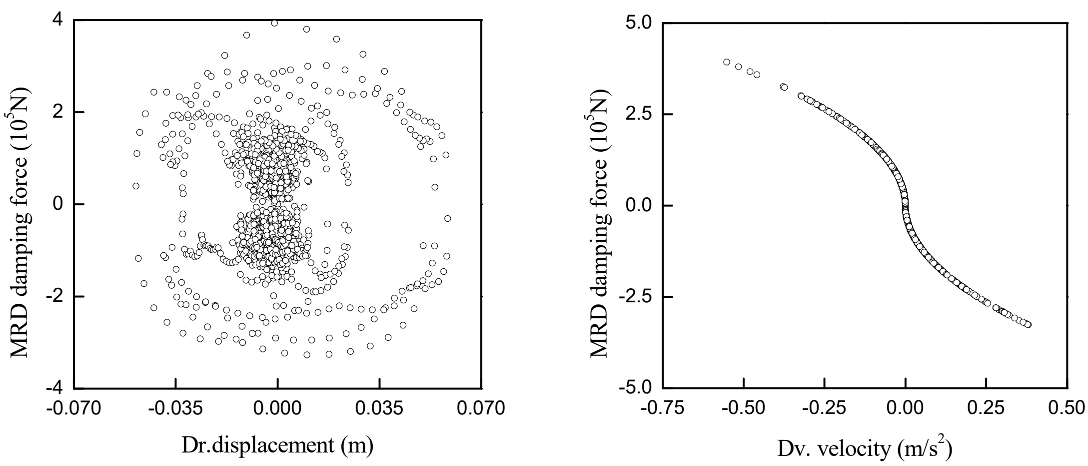

(a) Damping force versus inter-story displacement (b) Damping force versus velocity

Fig. 10 MRD damping force versus inter-story displacement and velocity under EI Centro seismic excitation

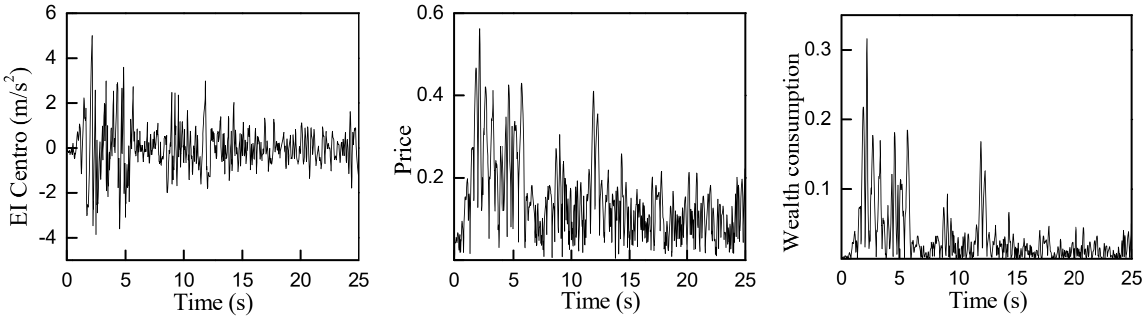

(a) El Centro acceleration time history (b) Price time history (c) Wealth consumption history

Fig. 11 Comparison of results among time histories

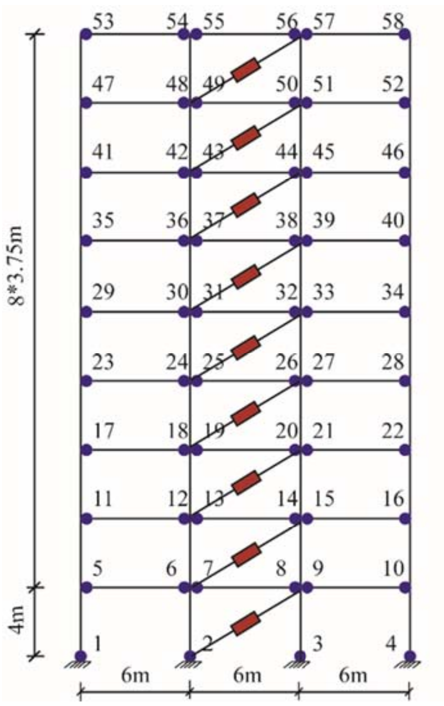

Fig. 12 Distribution of plastic hinges

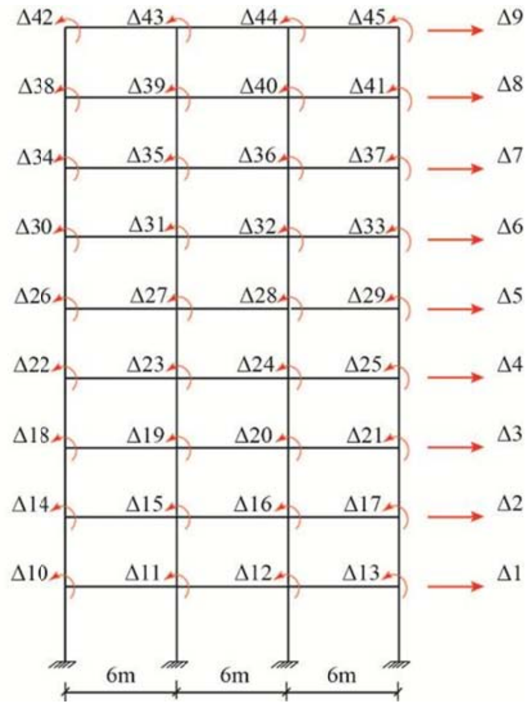

Fig. 13 Numeration of structural degree of freedom

4.2 A 9-story structure

To verify the effectiveness and superiority of the nonlinear MBC robust strategy, the approach is applied to a 9-story steel frame structure (Zhao *et al*. 2006) and compared to the nonlinear H_∞ robust control strategy. The mass of each floor is 1.08×10^5 kg. Some parameters are shown in Table 4.The damping ratio is ζ=0.02, and the elastic modulus is 2×10^5 N/mm^2. Positions of plastic hinges of structure are shown in Fig. 12, and the degrees of freedom are depicted in Fig. 13. The input ground motion records are El Centro (NS, May, 18, 1940) and Kobe (NS, Jan 17, 1995), and the peak accelerations are scaled to 500 gal with a duration of 35 s.

Table 4 Main parameters of nine-story steel frame structure

Structural component	Elastic modulus EI(N×m^2)	Yielding moment M(N×m)
1st to 3rd rows columns	2.31×10^8	1.97×10^6
4th to 6th rows columns	1.59×10^8	1.53×10^6
7th to 9th rows columns	1.47×10^8	1.41×10^6
1st to 3rd rows beams	2.38×10^8	1.53×10^6
4th to 6th rows beams	2.10×10^8	1.27×10^6
7th to 9th rows beams	1.44×10^8	1.05×10^6

Table 5 The response and control effects of the top story

Earthquake record	Case	Inter-story drift		Absolute acceleration		Time consumed (s)
		Peak (cm)	Reduction rate (%)	Peak (m/s^2)	Reduction rate (%)	
El Centro	FREE	2.66	—	13.44	—	—
	R-H$_\infty$	1.25	53.01	10.14	24.55	6.42
	R-MBC	0.88	66.92	8.84	34.23	1.93
Kobe	FREE	2.71	—	10.68	—	—
	R-H$_\infty$	1.86	31.37	6.39	40.17	5.86
	R-MBC	1.35	50.18	5.49	48.60	1.30

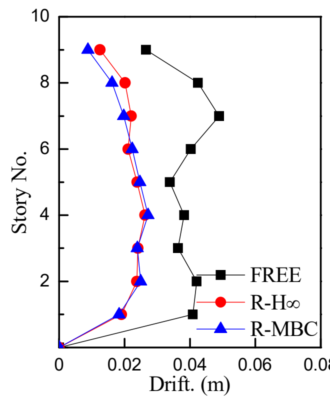

(a) Inter-story drift

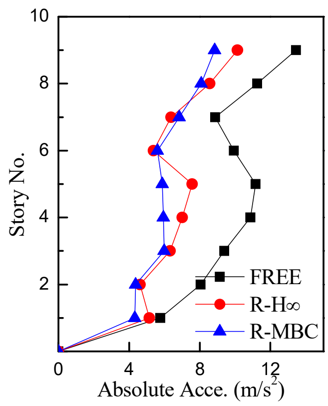

(b) Absolute acceleration

Fig. 14 The maximum relative displacement of each story during El Centro earthquake

The determination of controller parameters can be obtained from Eq. (16). The gain factor K=1200000, $\boldsymbol{\alpha}$=diag([0.36, 0.30, 0.34, 0.29, 0.28, 0.28, 0.27, 0.23, 0.30]) and $\boldsymbol{\beta}$=diag([3.61, 2.96, 3.4, 2.86, 2.85, 2.76, 2.7, 2.26, 2.97]). The induced norm of the uncertain part of system can be determined by the extended W-W algorithm. Table 5 lists the peak response and decreasing amplitude ratio of the 9th floor of the structure when subjected to El Centro and Kobe earthquake excitations. It can be seen that the R-MBC and R-H$_\infty$ strategies both achieved good control effectiveness. For the El Centro wave, the former strategy has a decreasing amplitude ratio of

66.92%, and the latter is 53.01%; the computation time of former strategy is 69.94% faster than that of the latter strategy. For the Kobe wave, the former strategy has a decreasing amplitude ratio of 50.18%, and the latter is 31.37%; the computation time of former strategy is 77.82% faster than that of the latter strategy for the El Centro wave. This is because the R-MBC requires only multiplication when calculating the gain matrix, whereas the nonlinear robust optimal control needs the complicated iterative process for solving the Riccati equations. The control effect of the R-MBC is better than the R-H_∞ in terms of the absolute acceleration under the actions of two earthquake waves. To illustrate the clear control effect of two cases, Fig. 14 shows the maximum relative displacement of each story. Fig. 14(a) is the inter-story drift of each floor, and Fig. 14(b) is the absolute acceleration of each floor. The control effect of the R-MBC is also better than the R-H_∞ when using the same approach to address the uncertainty of the system because the R-H_∞ strategy is time invariant and has an insufficient capacity to change according to working conditions. However, the control force of the R-MBC is determined by the supply and demand in the virtual market, which determines the price of virtual market. Thus, price fluctuations lead to changes in the gain matrix of the controlled system, which means that the control energy can be distributed reasonably in every moment. Besides, the H_∞ norm which can be obtained by the extended W-W and precise integration method is introduced into the MBC system, and then the calculation of the induced norm can be transferred to the calculation of interval matrix and eigenvalue.

Fig.15 shows the rotations curves versus the time history of the 5th PHL under the El Centro seismic excitation. The uncontrolled structure has entered the plastic stage, and the FAM can detect the order and size of plastic hinges when they occur. Fig. 16 exhibits the MRD damping force versus the inter-story displacement and velocity under the El Centro seismic excitation. It can be seen that the MRD output force has a stronger correlation with the inter-floor relative velocity than that with the inter-floor relative displacement, and the MRD damping force lies in the opposite direction of relative velocity. Moreover, the R-MBC performs better than the R-H_∞ in realizing the opposite damping force to the inter-floor relative velocity, so the R-MBC is more suitable for the MRD semi-active control strategy.

Fig. 17 shows the structural energy response with the R-H_∞ and R-MBC strategies under the El Centro seismic excitation. IE, CE, KE, DE and SE are total energy inputted by ground motions, dissipated energy of the control device, kinetic energy of the system, damping energy and elastic

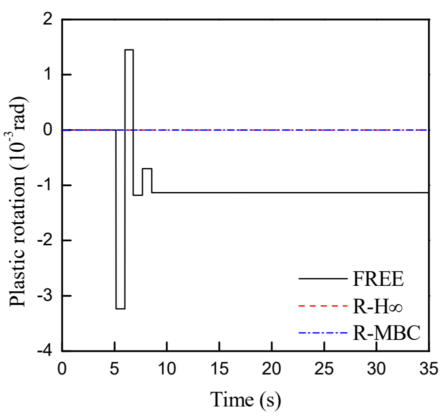

Fig. 15 Rotation curves versus time history of the 5th PHL under El Centro seismic excitation

potential energy, respectively. Fig. 17(c) indicates that the total dissipated energy required from the control device is almost the same under the R-H_∞ and R-MBC. Figs. 17(a)-(b) depict the energy response time history of structure for two working cases. It can be seen that most of input energy has been dissipated by the MRD control device when it is in use, and the kinetic energy, elastic energy and damping energy decreased. From Table 5 and Fig. 17, the energy response time history is almost the same under the R-H_∞ and R-MBC. However, the control effect of the R-MBC algorithm is better than that of the R-H_∞ algorithm, which proves the effectiveness of the R-MBC algorithm.

In conclusion, the R-H_∞ is an optimal control algorithm based on the full state feedback, and its effectiveness is dependent on the accurate feedback of full state. This algorithm might have a time delay and long online time when there are many degrees of freedom. However, the R-MBC

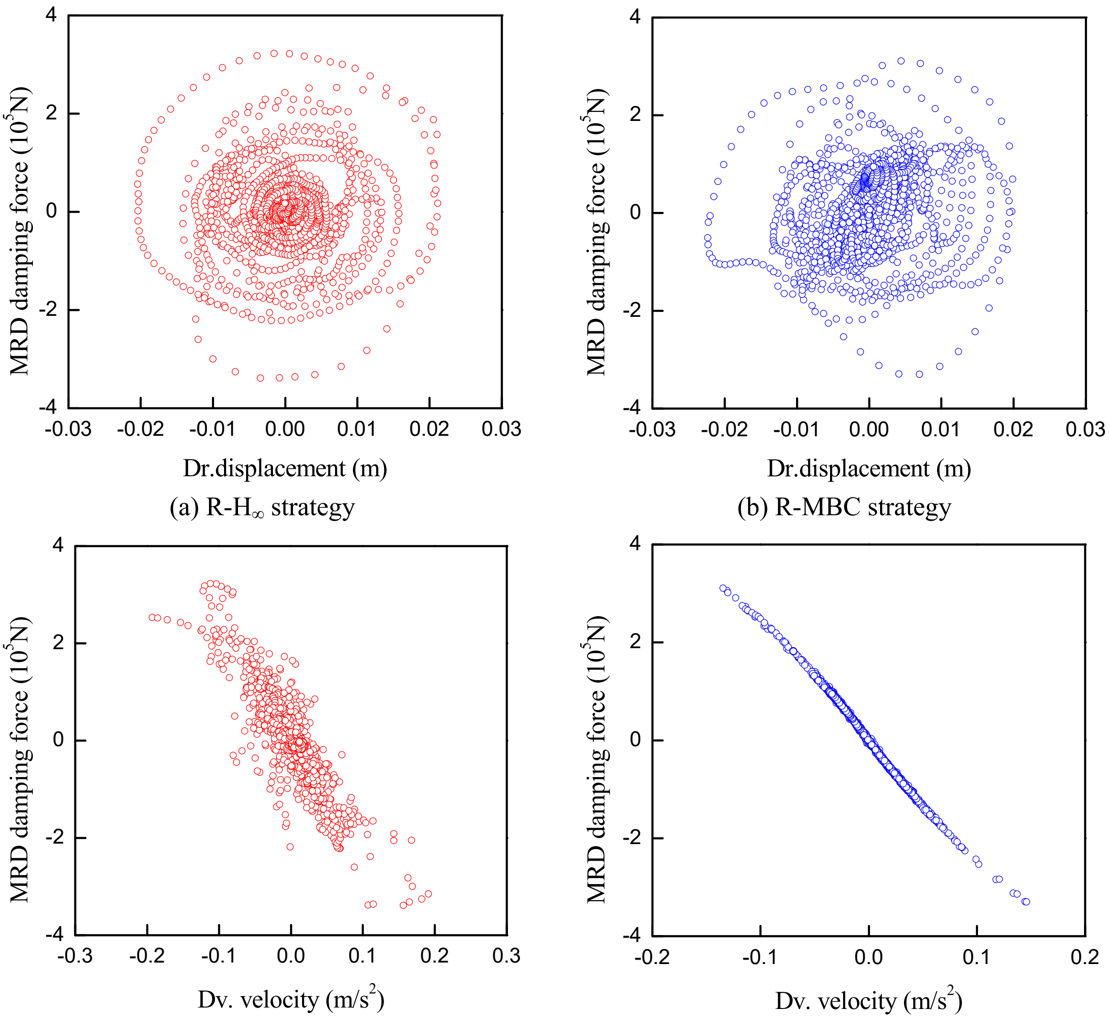

(a) R-H_∞ strategy (b) R-MBC strategy

(c) R-H_∞ strategy (d) R-MBC strategy

Fig. 16 MRD damping force versus inter-story displacement and velocity under El Centro seismic excitation

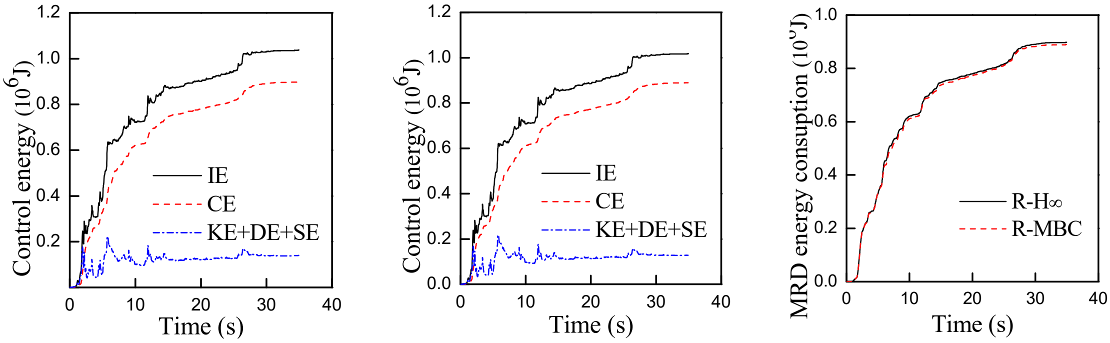

(a) R-H$_\infty$ strategy (b) R-MBC strategy (c) Comparison

Fig. 17 Structural energy response with R-H$_\infty$ and R-MBC strategy under El Centro seismic excitation. Solid green line: IE (input seismic energy), dashed pink line: CE (control energy), dotted black line: KE (kinetic energy) + DE (potential energy) + SE (damping energy)

requires only the information of discrete layer. That is, it gives the static discrete Pareto optimal control of response of discrete layer to realize the optimal control of the whole system. The R-MBC requires less information and short computational time, which can eliminate the impact of time delay. The numerical example demonstrates that the R-MBC can achieve a better control effect than the R-H$_\infty$ strategy in terms of nonlinear robust control since it has the advantage of a simple parameter determination process for controller parameters, independence of global variables and ease of use.

5. Conclusions

The demand for the control force based on the R-MBC depends on the equilibrium price that controls energy because its strategy takes advantage of the market price lever concept. To some extent, the time history has a relationship with external excitations such that the R-MBC strategy performs well in reflecting the impact of an input on the controlled system and has a good adaptability. The numerical examples of the 1-story and 9-story buildings with the MRD devices further demonstrate the effectiveness of the proposed R-MBC algorithm. The approach has the advantage of simple parameter determination and short online computation time, which provides a reference on its practical application. The following conclusions were drawn throughout the numerical simulation analysis.

• The present study uses the computational structural mechanics and optimal control theory to determine the uncertainty of systems by introducing the induced norm into the MBC system. The induced norm is the elastic stable Euler critical force, and smaller than the critical value rather than close to the critical value.

• The FAM is introduced into the linear MBC robust system to enhance the computation efficiency of the nonlinear robust control system. The numerical examples of the 1-story and 9-story buildings with the MRD devices demonstrate that the FAM could capture the order and value of plastic hinge for each moment.

• This paper introduces the induced norm with the FAM to design a nonlinear MBC robust controller. The numerical examples indicate that the R-MBC has a better control effect than the

R-H_∞ when the control energy is the same, and prove the effectiveness of the proposed strategy.

• The energy price mechanism in the MBC theory can reflect the change in the control force demand when the structure is subjected to earthquakes and reflect the influence of input energy on the output force of a controlled system.

Acknowledgments

The research described in this paper was financially supported by the National Natural Science Foundation of China under Grant Nos. 51261120375 and 51421064.

References

Aloliwi, B. and Khalil, H.K. (1997), "Robust adaptive output feedback control of nonlinear systems without persistence of excitation", *Automatica*, **33**(11), 2025-2032.

Baskar, J. and Bradley, R.H. (1994), "An optimization approach to robust nonlinear control design", *Int. J. Control*, **59**(3), 639-664.

Cho, H.C., Jin, W.L., Lee, Y.J. and Lee, K.S. (2008), "Lyapunov theory based robust control of complicated nonlinear mechanical systems with uncertainty", *J. Mech. Sci. Technol.*, **22**(11), 2142-2150.

Hrovat, D., Barak, P. and Rabins, M. (2014), "Semi-active versus passive or active tuned mass dampers for structural control", *J. Eng. Mech.*, **109**(3), 691-705.

Huo, L.S. and Li, H.N. (2005), "Control law for market-based semi active tuned liquid column dampers", *J. Appl. Mech.*, **22**(1), 71-75.

Katebi, M.R., Grimble, M.J. and Zhang, Y. (1997), "H∞ robust control design for dynamic ship positioning", *Iee. P-contr. Theor. Appl.*, **144**(2), 110-120.

Kuperman, A. and Zhong, Q.C. (2011), "Robust control of uncertain nonlinear systems with state delays based on an uncertainty and disturbance estimator", *Int. J. Robust Nonlin.*, **21**(1), 79-92.

Kushner, H.J. (2006), "Numerical approximations for non-zero-sum stochastic differential games", *Siam. J. Control Optim.*, **46**(6), 1942-1971.

Li, G., Liu, Q.F. and Li, H.N. (2011), "Inelastic structural control based on MBC and FAM", *Math. Prob. Eng.*, **11**(1): 1-18.

Li, G., Zhang, Y. and Li, H.N. (2014), "Nonlinear seismic analysis of reinforced concrete frames using the force analogy method", *Earthq. Eng. Struct.*, **43**(14), 2115-2134.

Li, H.N. and Li, Y. (2008), "Semi-active control for MRD-isolation structure using MBC strategy", *J. Earthq. Eng. Vib.*, **28**(5), 140-145.

Lin, T.H. and Pian, T. (1969), "Theory of inelastic structures", *J. Appl. Mech.*, **287**(4), 354-355.

Liu, X., Su, H., Yao, B. and Chu, J (2009), "Adaptive robust control of nonlinear systems with dynamic uncertainties", *Int. J. Adapt. Control Sig. Proc.*, **23**(4), 353-377.

Luo, Y., Sun, Q., Zhang, H. and Cui, L. (2015), "Adaptive critic design-based robust neural network control for nonlinear distributed parameter systems with unknown dynamics", *Neurocomputing*, **148**, 200-208.

Lynch, J.P. and Law, K.H. (2002), "Market-based control of linear structural systems", *Earthq. Eng. Struct.*, **31**(10), 1855-1877.

Lynch, J.P. and Law, K.H. (2004), "Decentralized energy market-based structural control", *Earthq. Eng. Struct.*, **17**(3-4), 557-572.

Marino, R. and Tomei, P. (1997), "Nonlinear control design", *Automatica*, **33**(9), 1769-1770.

Peng, H., Wu, Z.G. and Zhong, W.X. (2014), "H_∞ norm computation of linear continuous-time periodic systems by a structure-preserving algorithm", *Int. J. Control*, **87**(1), 131-142.

Safonov, M.G., Chiang, R.Y. and Flashner, H. (1991), "H (infinity) robust control synthesis for a large space

structure", *J. Guid., Control, Dyn.*, **14**(3), 513-520.
Tan, S.J., Wu, Z.G. and Zhong, W.X. (2008), "Optimal induced norm computation of discrete H_∞ control systems with time-delays", *J. Global. Optim.*, **40**(4), 653-662.
Wang, C.L. and Lin, Y. (2013), "Robust adaptive neural control for a class of uncertain MIMO nonlinear systems", *Int. J. Syst. Sci.*, **46**(11), 1-10.
Wanxie, Z., Williams, F.W. and Bennett, P.N. (1997), "Extension of the Wittrick-Williams algorithm to mixed variable systems", *J. Vib. Acoust.*, **119**(3), 334-340.
Wong, K.K. (2005), "Predictive optimal linear control of inelastic structures during earthquake. Part II", *J. Eng. Mech.*, **131**(2), 142-152.
Wong, K.K. and Zhao, D.F. (2007), "Uncoupling of potential energy in nonlinear seismic analysis of framed structures", *J. Eng. Mech.*, **133**(10), 1061-1071.
Wu, Z.G. and Zhong, W.X. (2009), "A structure-preserving algorithm for the minimum H_∞ norm computation of finite-time state feedback control problem", *Int. J. Control*, **82**(4), 773-781.
Zhang, Y.G., Xiang, J. and Xiao, J. (2004), "Decentralized stabilization of continuous-time fuzzy large-scale systems via LMI method", *Syst. Eng. Electron.*, **26**(6), 773-776.
Zhao, G.W., Pei, X.Z. and Zhou, X.S. (2006), "The fundamental research on prediction method of structural earthquake response based on energy balance", *Ind. Constr.*, **36**(1), 182-187.
Zhong, W.X. (2004), "On precise integration method", *J. Comput. Appl. Math.*, **163**(1), 59-78.
Zhou, J. and Wen, C. (2011), "Robust adaptive control of uncertain nonlinear systems in the presence of input saturation", *Syst. Indent.*, **56**(7), 1672-1678.

CC